Investigation of the potential of Interferometric Synthetic Aperture Radar (InSAR) to detect land subsidence in SW Utah

by

Richard R. Forster

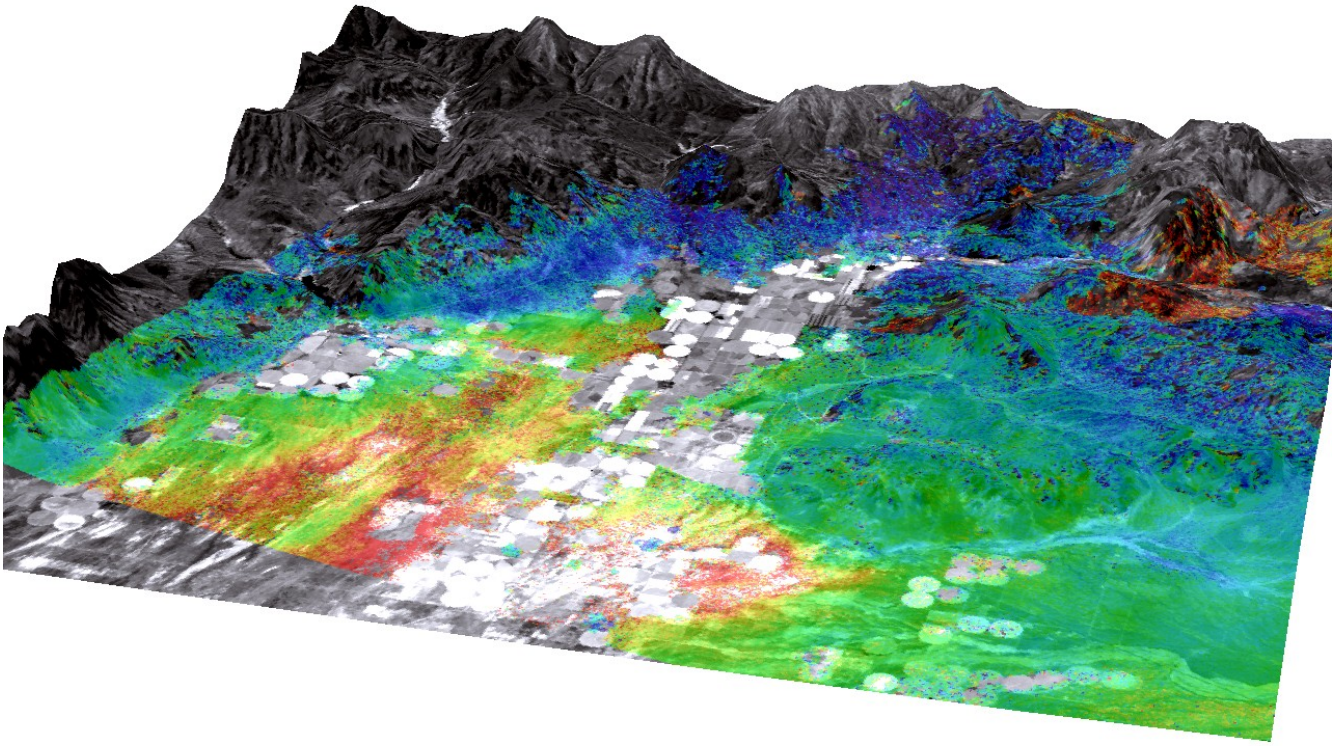

OPEN-FILE REPORT 446 **January 2005**
UTAH GEOLOGICAL SURVEY
a division of
UTAH DEPARTMENT OF NATURAL RESOURCES

This Open-File Report represents material that may not have undergone policy, technical, or editorial review required for other UGS publications. It provides information that, in part, may be interpretive or incomplete and readers are to exercise some degree of caution in the use of the data. Although this product represents the work of professional scientists, the Utah Department of Natural Resources, Utah Geological Survey, makes no warranty, stated or implied, regarding its suitability for a particular use. The Utah Department of Natural Resources, Utah Geological Survey, shall not be liable under any circumstances for any direct, indirect, special, incidental, or consequential damages with respect to claims by users of this product.

Investigation of the potential of Interferometric Synthetic Aperture Radar (InSAR) to detect land subsidence in SW Utah

Submitted to the Utah Geological Survey in fulfillment of contract #056175

by Richard R. Forster

January 18, 2005

Objective

The objective of this study is to evaluate the potential of Interferometric Synthetic Aperture Radar (InSAR) to measure land surface change in southwest Utah. This study is referred to as Phase-1. Based on the results of Phase-1 and the desires of the Utah Geological Survey, Phase-2 would be the implementation of this technique over a longer time frame with a more extensive InSAR data set.

Data set

Synthetic aperture radar (SAR) data acquired by the European Space Agency's ERS-1 were used to assess the ability of interferometric SAR (InSAR) to detect surface change in SW Utah. This report (Phase 1) utilized ERS-1 data freely available to the research community. Coverage of SW Utah was limited to 4 scenes (100 x 100 km each). Figure 1 shows the SAR frame boundary on a Landsat ETM+ scene. bands, date, path row, source scene. Details of the Utah portion of the frame are shown in Figure 2.

Phase-2 data will be available from ESA either by purchase at full price for commercial applications or through a research oriented data grant at reduced cost. The data grants are awarded based on a proposal which can take several months for evaluation. A proposal to ESA has already been submitted for Phase 2 of this project in order to reduce the time required to obtain the data should Phase-2 be pursued.

The four ERS-1 SAR scenes used in Phase-1 are summarized in Table 1. These four scenes can be combined to yield six different interferometric pairs each producing an interferogram or fringe image. The interferograms are characterized by their temporal and spatial baselines. The temporal baseline is the amount of time between the two SAR acquisitions. (ERS-1 has a repeat orbit of 35 days). The spatial baseline is the distance between the two orbit paths at the time of acquisitions. The shortest possible spatial baseline is desirable for displacement measurements as the undesirable influence of topography is reduced. The temporal and spatial baselines for the six pairs are listed in Table 2.

Acquisition date	Orbit	Frame
06/11/1992	04738	2853
08/20/1992	05740	2853
04/15/1995	19611	2853
11/11/1995	22617	2853

Table 1. Acquisition dates, orbits, and the frame for the four ERS-1 SAR scenes used in this study.

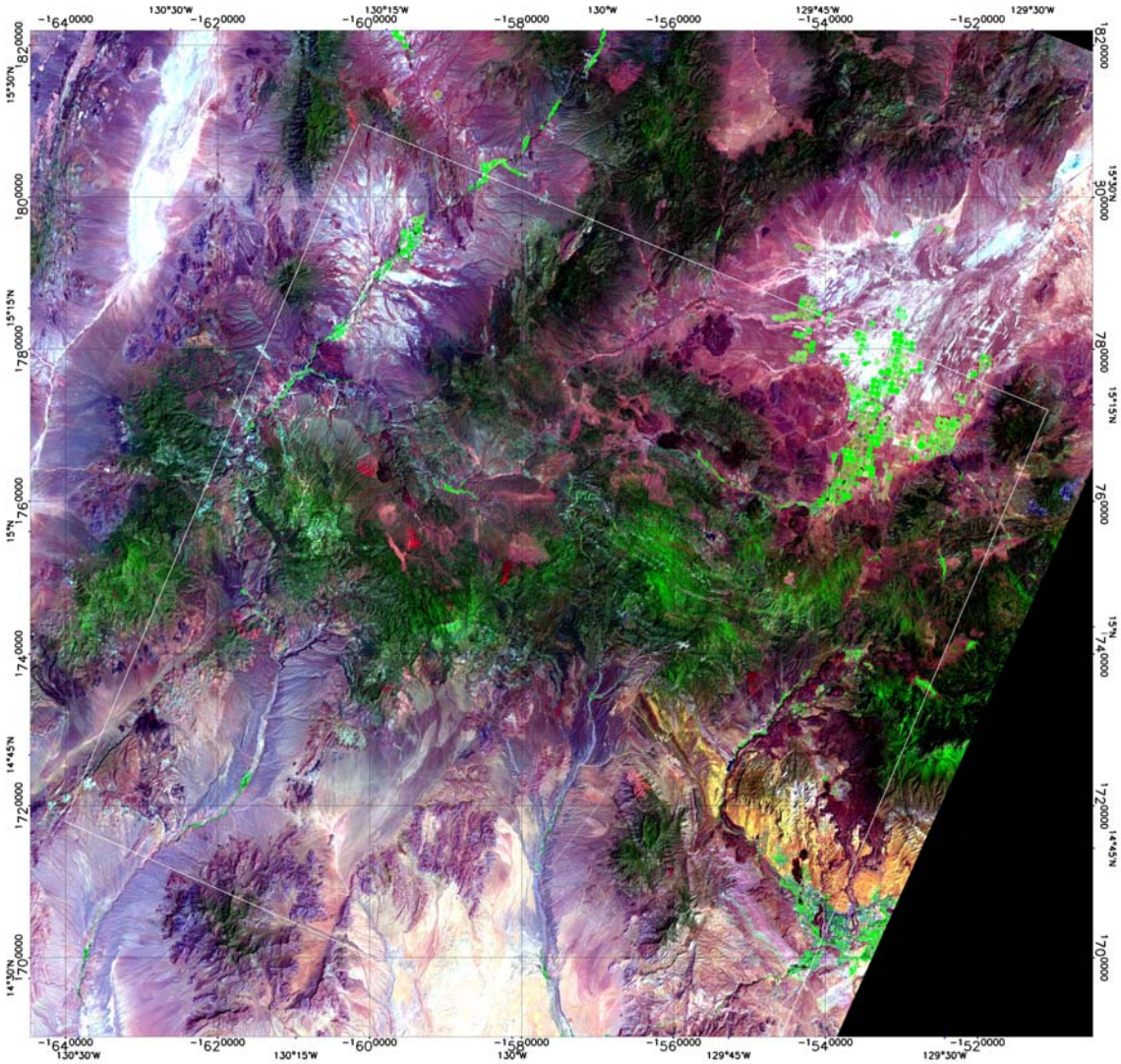

Figure 1. Landsat ETM+ scene acquired 06/13/2000 (path 39, row 34) red: band 7, green: band 4, blue: band 2. The white box is the approximate location of the SAR frame.

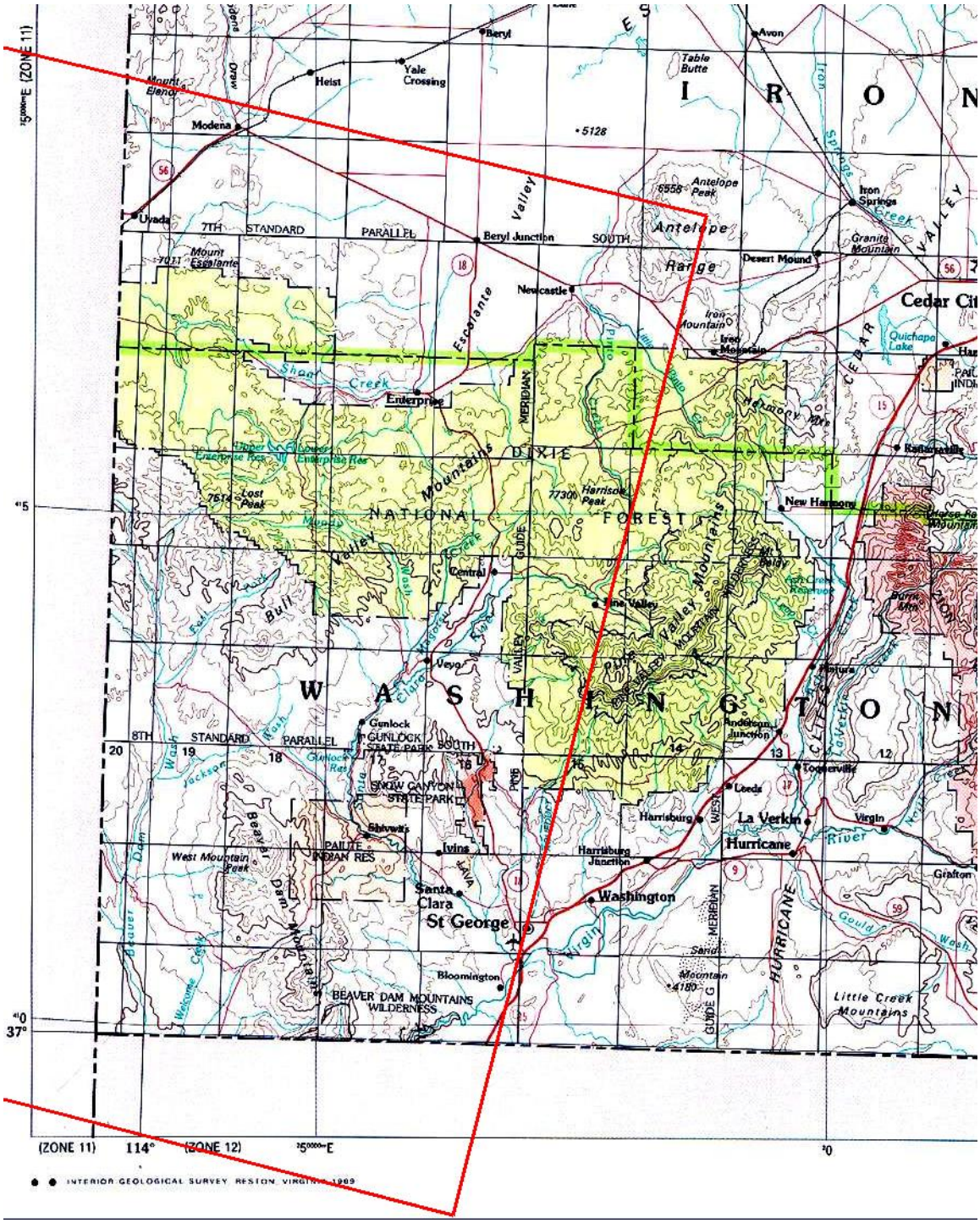

Figure 2. Southwest corner of Utah with red box indicating approximate location of SAR frame.

Acquisition date	*08/20/1992*	*04/15/1995*	*11/11/1995*
06/11/1992	376 m, 2 mths.	411 m, 2 yrs. 10 mths.	52 m, 3 yrs. 5 mths.
08/20/1992		35 m, 2 yrs. 8 mths	324 m, 3 yrs. 3 mths
04/15/1995			359 m, 7 mths.

Table 2. Spatial and temporal baselines for the paired SAR acquisitions used to form the six interferograms.

The six baselines available from the four acquisitions provide a variety of combinations of both spatial and temporal baselines. Two of the pairs produce a short temporal baseline with long spatial baselines, two have a short spatial baseline and long temporal baseline, and the other two have a long temporal and long spatial baseline (Figure 3). This variability in baselines will aid in the evaluation of the baseline constraints for Phase-2 of the project. In order to place the temporal baselines in a chronological setting they are also shown in timeline format (Fig. 4). The color of the line segment representing the temporal baselines is used again in latter figures to cross reference the InSAR products with their corresponding baselines and acquisition timing.

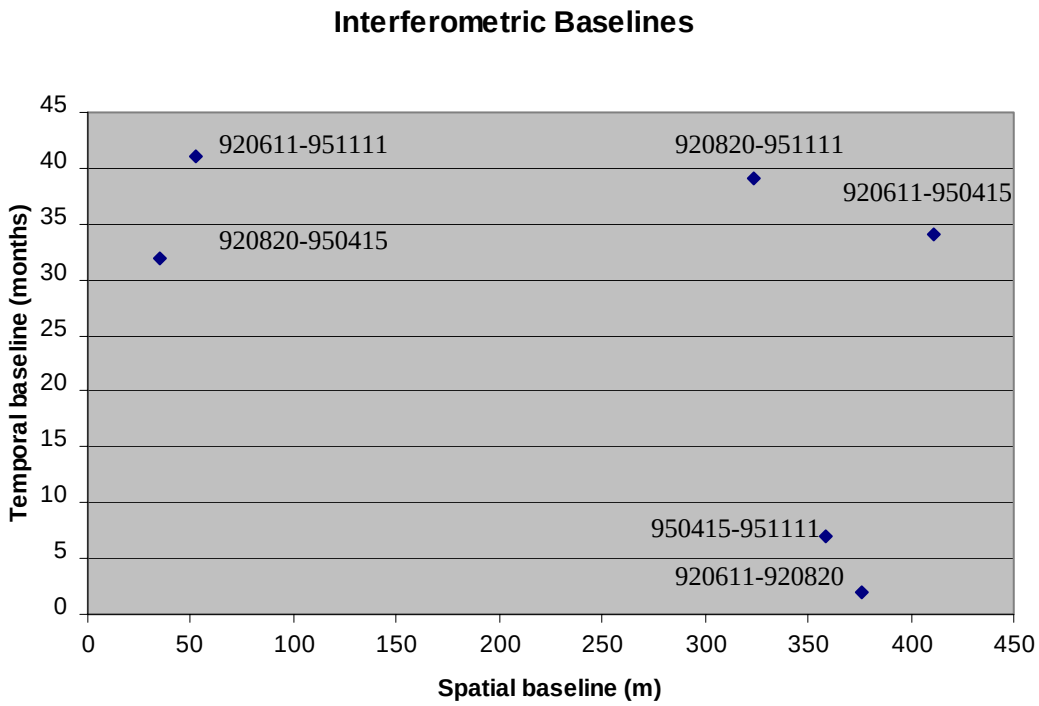

Figure 3. Temporal and spatial baselines for the six pairs of SAR acquisitions.

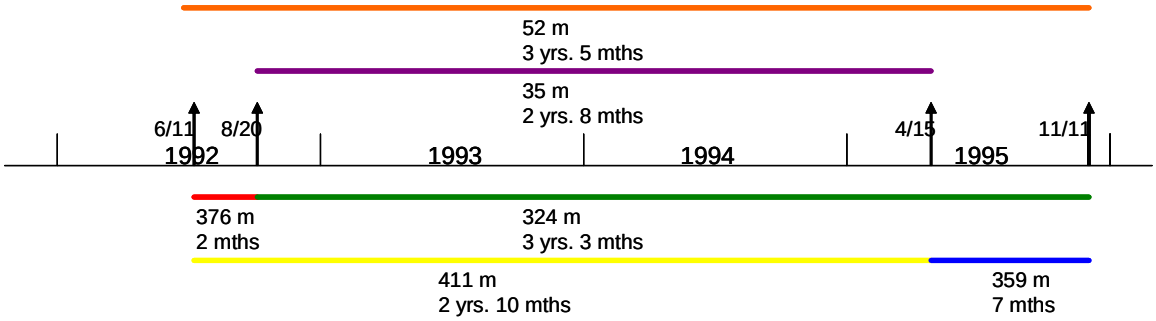

Figure 4. Time line showing the acquisition dates, temporal and spatial baselines of the six InSAR pairs used in this study.

Processing

The data processing was done using programming modules from specialized SAR and InSAR software written by Gamma Remote Sensing. Customized Unix scripts were written to execute the Gamma commands required for this project.

The four raw ERS-1 SAR scenes were obtained from a consortium of universities archive. Enhanced orbital tracking data were downloaded from the University of Delft, The Netherlands, web site for each scene. The four scenes were processed using these precision orbits to a single-look-complex (SLC) image format where each 8 x 4 m pixel is represented by an amplitude and phase of the returned radar pulse. The six SLCs pairs were coregistered to each other with the pixel-scale offset manually determined by selecting ground control points in each image using ENVI image processing software.

More precise offsets were determined using correlation matching to $1/10^{th}$ of a pixel. The first scene acquired for each pair was designated as the *master* with the most recent of the pair being the slave. Each slave SLC was coregistered to its corresponding master SLC and resampled. The phase for each pixel of the master was subtracted from the reseampled phase of the slave to form an interferogram for all six pairs. Coherence images for each pair were also formed representing the local spatial homogeneity of the phase in the interferogram. The higher coherence regions (bright areas in the image) represents a more reliable phase measurement.

At this point in the processing the phase of the interferogram is due to topography, the spatial baseline, and any surface displacement occurring between SAR acquisitions. There is also the possibility of differences in atmospheric path delays due to changes in water vapor content during the two acquisitions. This can cause an unwanted phase signal that is best removed using a long time series of interferograms ($n > \approx 10$). Standard processing removes the phase contribution from the spatial baseline and topography by simulating an interferogram using a DEM of the area and the precision orbits of the two passes of the satellite. This synthesized phase image is subtracted from the phase of the interferogram, theoretically leaving only the phase due to surface displacement. This was done for each of the six interferograms yielding six differential interferograms.

Some of the differential interferograms had a periodic phase structure left in them due to inexact estimation of the spatial baseline. This was removed by estimating the residual baseline from the period of the phase pattern using a Fast Fourier Transform (FFT) of the interferogram. The estimated residual baseline was used to form another synthetic phase image along with the DEM. This simulated phase image was also subtracted from the original interferogram further removing the effects of the spatial baseline, isolating the surface displacement component.

Georeferencing and projection transformation were done on the SAR, Landsat and DEM so they could be co-located at a 30-m pixel scale. The SAR power images, coherence images and interferograms, were all geocoded by transforming from SAR coordinates to UTM zone 12, with a NAD 1927 geoid. The Landsat ETM+ scene was reprojected from Albers to UTM and resampled to match the geocoded InSAR images. The DEM used was acquired from the USGS as part of their Seamless Data Distribution. The source of this DEM was the NASA SRTM which has 30 m pixels, but some data gaps in areas of high topographic relief. The missing data were filled using an spatial interpolation routine in ENVI. The SAR and InSAR data products are all terrain corrected and ortho-rectified using the DEM.

Results and Analysis

The four SAR geocoded terrain-corrected power images are all similar in their general pattern of radar return throughout most of the scene. Three of these images are shown in Figure 5 along with a color composite image highlighting the isolated areas of subtle change between the acquisitions. The color image (Fig. 5d) has the first three SAR images assigned to red, green, and blue respectively. The majority of the scene is dominated by shades of gray, indicting the power returned is unchanged for the three acquisitions used in the composite. The south end of the Escalente Valley (NE portion of the scene) is highlighted by colored agricultural fields. The presence of the color is due to a difference in power for at least one of the acquisitions. Most of the fields are green or yellow. Green is caused by a dominating a bright return on 920820, with yellow (absence of blue) indicating equally strong return on 920611 and 920820. Neither color has a significant contribution of blue, due to the relatively weak return from 950415. These colors correspond with the likely scenario of more mature crops in the fields during the summer months than in the spring. The fourth power image (951111, not shown) is similar to 950415, consistent with minimal crop bio-mass in late fall.

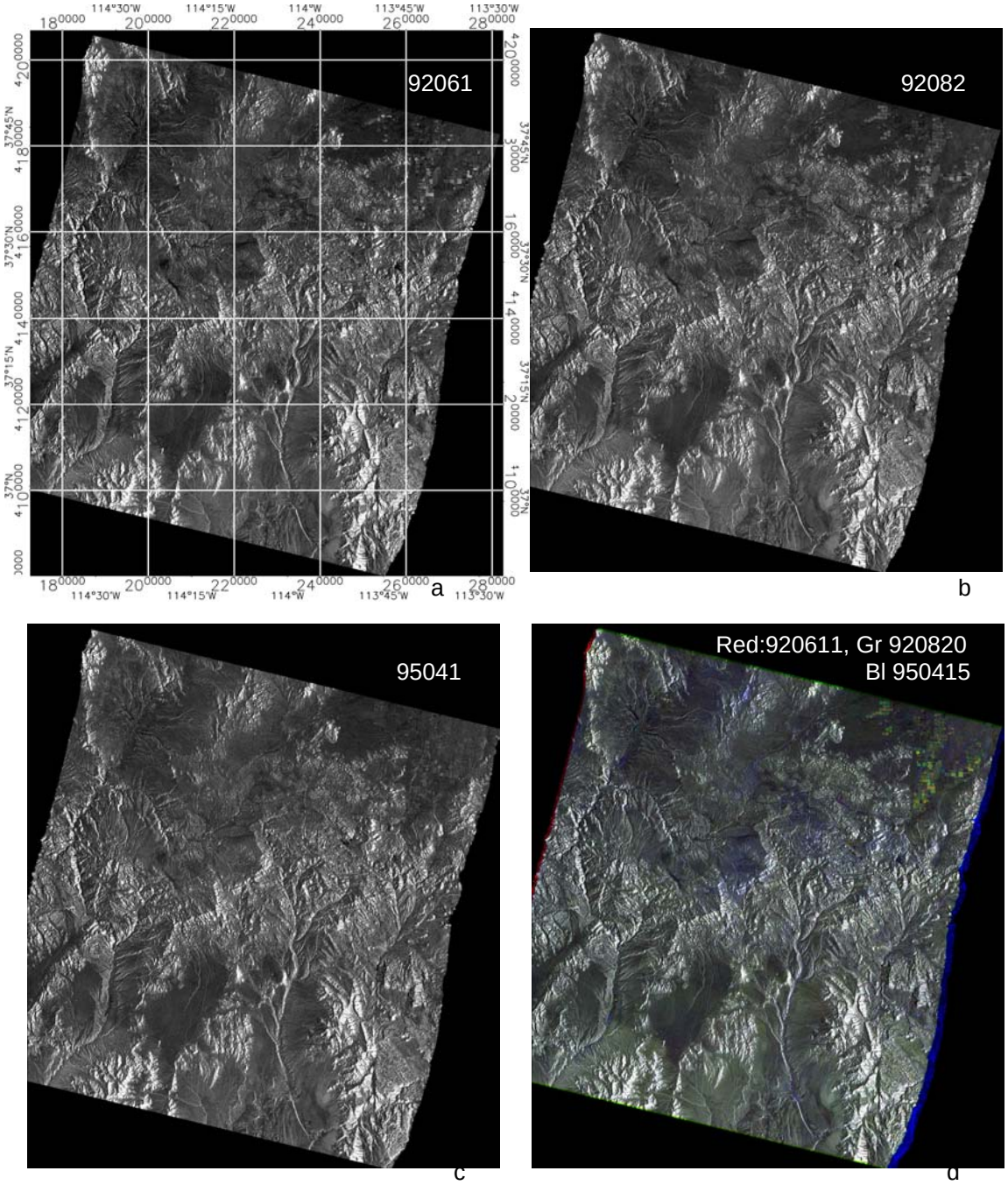

Figure 5. Geo-referenced and terrain corrected SAR power images a-c) of the first three acquisitions and d) a color composite.

The six interferograms and their corresponding coherence images are shown in Figure 6. The level of coherence and hence the quality of the phase signal varies considerably between the pairs and spatially within the images. In general, over the full extent of the scene, the areas with less vegetation have higher coherence when compared to the Landsat TM image (Fig. 1). This result is to be expected since the scattering surfaces of the vegetation (leaves and branches) are much less stable than those of exposed outcrops and bare soil. It appears that the only pair with unusable phase over a majority of the scene is one of the long spatial and temporal baseline pairs (Fig. 6b). Even this scene has adequate coherence in the south central portion of the image where there is minimal vegetation (Fig. 1).

The primary area of interest in this study is the agricultural region at the southern end of the Escalente Valley to the west of Newcastle, UT (Fig. 2). Coherence and fringe images centered on this region are shown in Figure 7. The areas immediately surrounding the center-pivot irrigated plots have relatively high coherence for the two short temporal baseline pairs (Figs. 7a and f). The other four pairs have poor phase information in these areas. This comparison is quantified by selecting a r*egion of interest* (ROI) around the irrigated plots (Fig. 7f) and computing a mean coherence value for each of the six pairs. Results of this analysis are listed in Table 3 below.

Acquisition dates	Temporal bsl.	Spatial bsl.	Mean coherence
920611-920820	2 mths.	376 m	0.29
920611-950415	2 yrs. 10 mths.	411 m	0.08
920611-951111	3 yrs. 5 mths.	52 m	0.01
920820-951111	2 yrs. 8 mths	35 m	0.11
920820-950415	3 yrs. 3 mths	324 m	0.09
950415-951111	7 mths.	359 m	0.18

Table 3. Spatial and temporal baselines for the paired SAR acquisitions and the mean coherence value in the region of interest (ROI) surrounding the agricultural areas. The location of the ROI is shown in Fig. 7f.

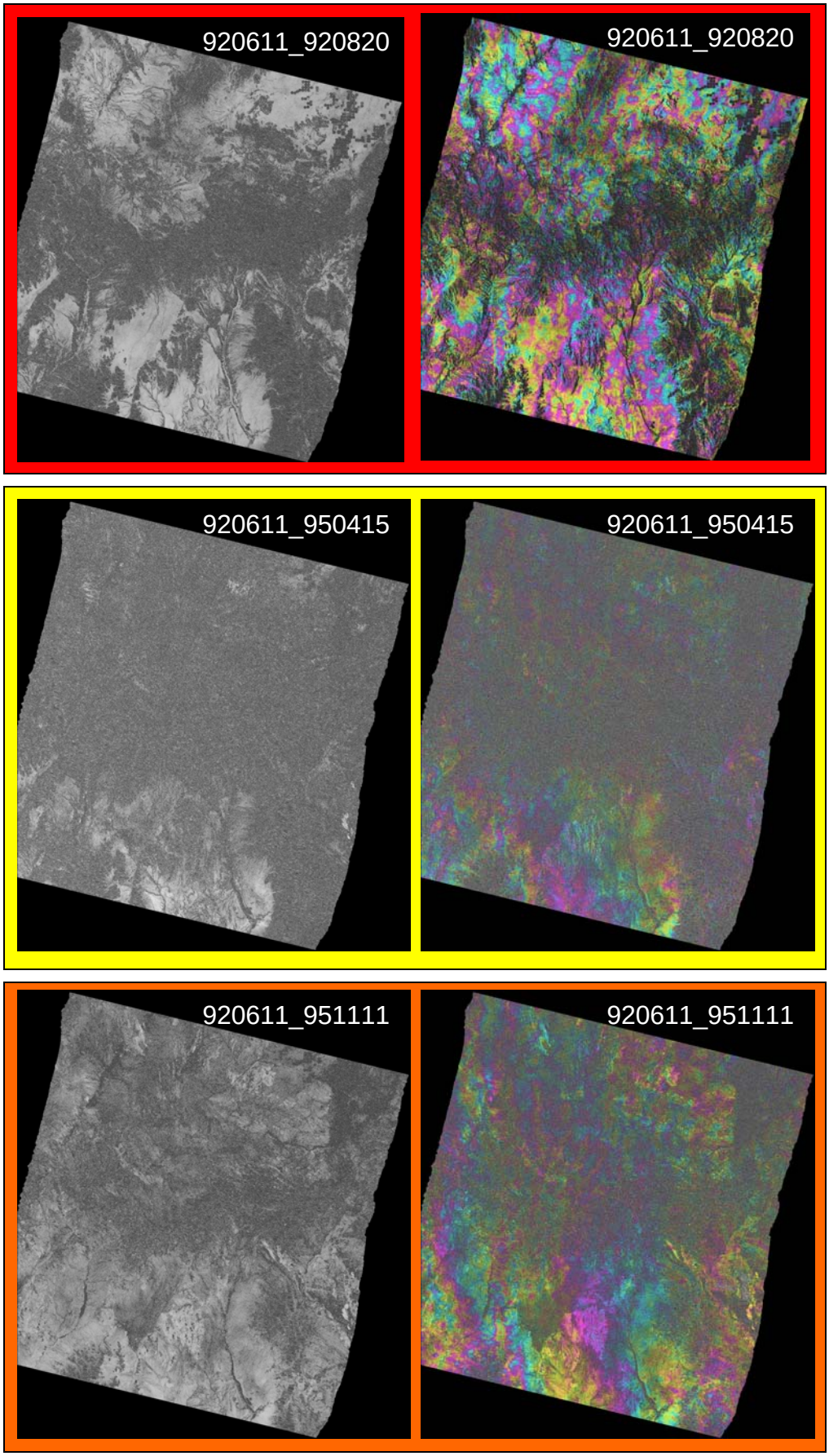

376 m
2 mths.
a.

411 m
2 yrs. 10 mths.
b.

52 m
3 yrs. 5 mths.
c.

Figure 6. Geo-referenced coherence images (left) and interferograms (right) of the full SAR scenes for the six InSAR pairs. Temporal and spatial baselines are to the right. Colored boxes correspond to the timeline colors in Fig. 4

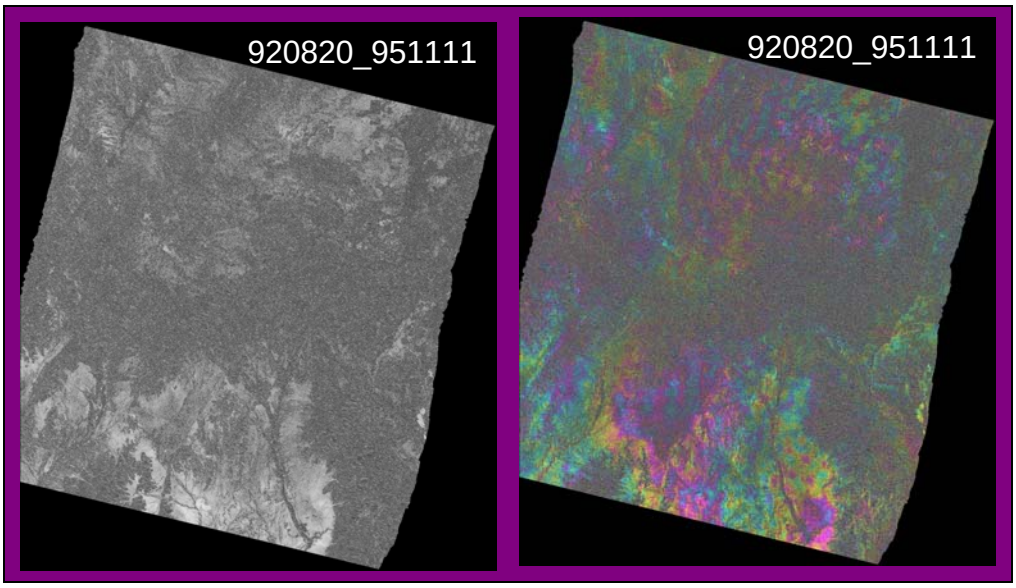

35 m
2 yrs. 8 mths.
d.

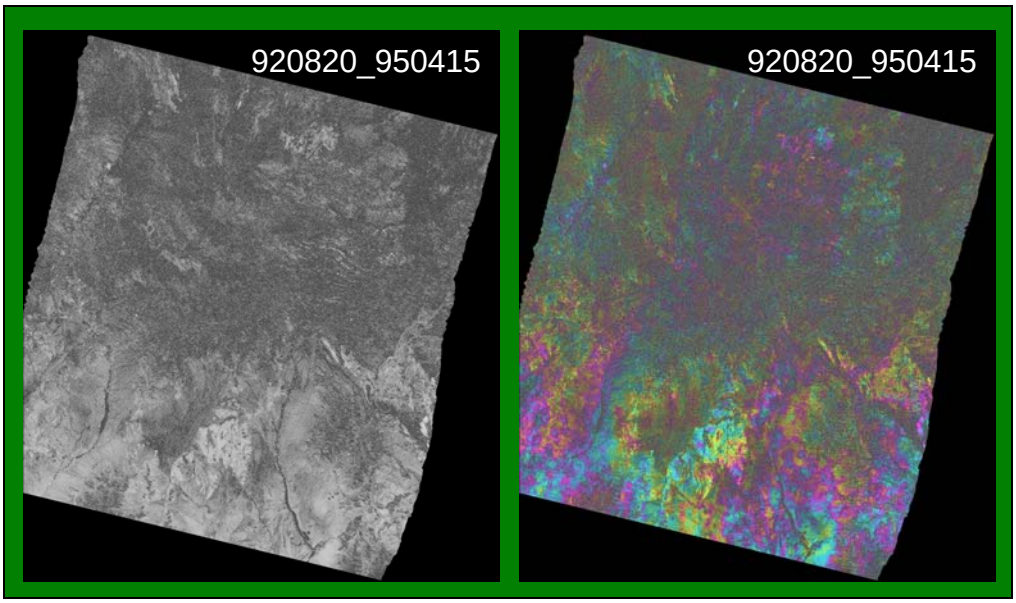

324 m
3 yrs. 3 mths.
e.

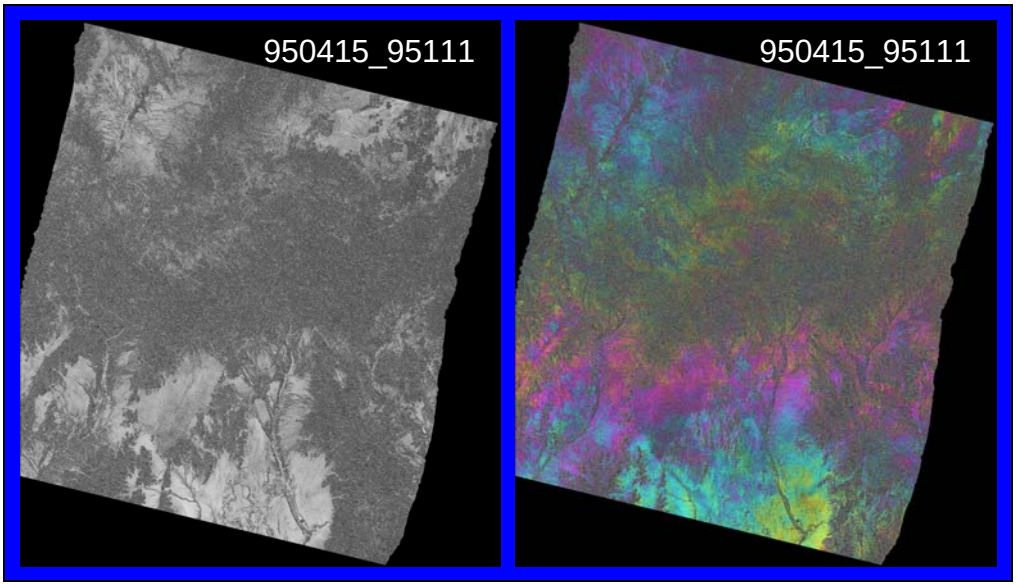

359 m
7 mths.
f.

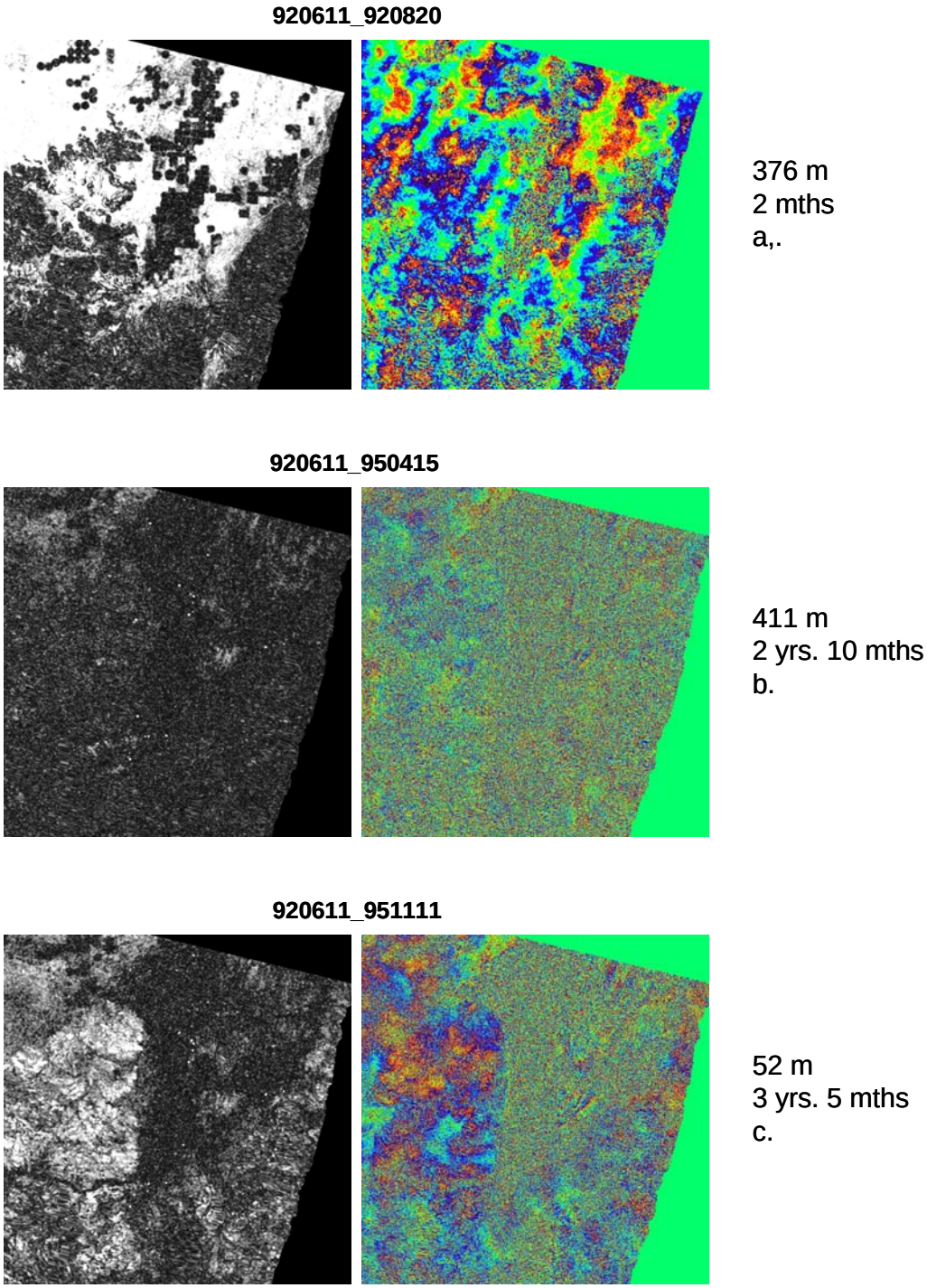

Figure 7. Geo-referenced coherence images (left) and interferograms (right) of the NE area for the six InSAR pairs. Temporal and spatial baselines are to the right. The agricultural area region of interest (ROI) is the red polygon in f.

920820_951111

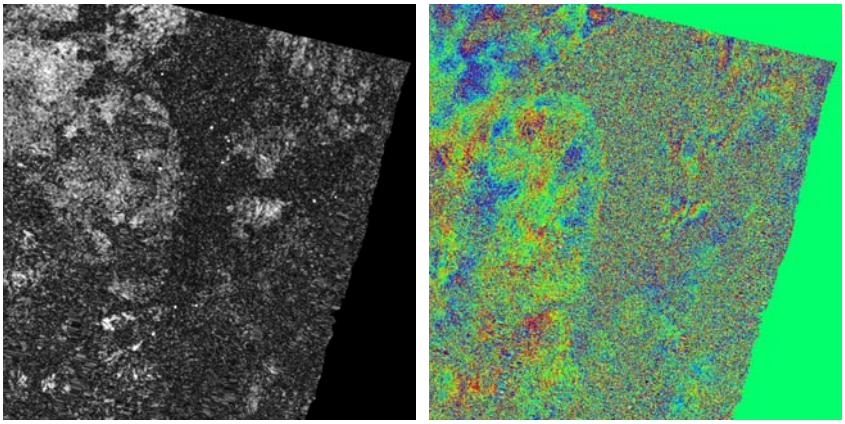

35 m
2 yrs. 8 mths
d.

920820_950415

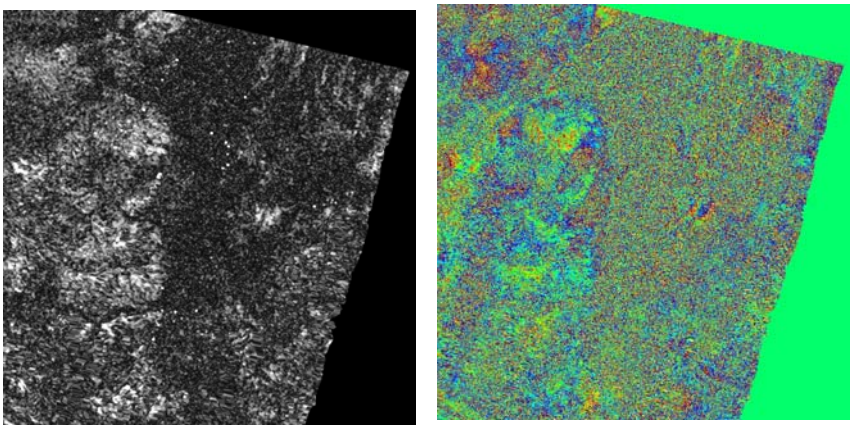

324 m
3 yrs. 3 mths
e.

950415_95111

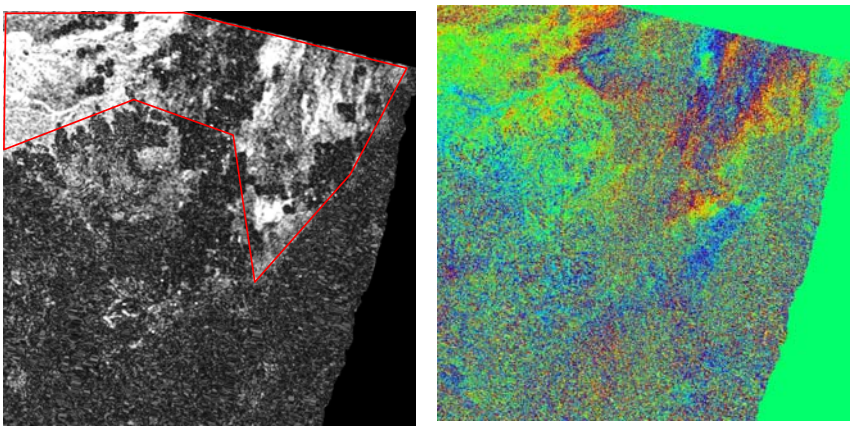

359 m
7 mths
f.

The influence of the baselines on the mean ROI coherence values are shown in the graphs below (Fig. 8). The spatial baseline appears to have no influence on the coherence of the agricultural area. However, the temporal baseline is strongly related to the coherence in this portion of the scene.

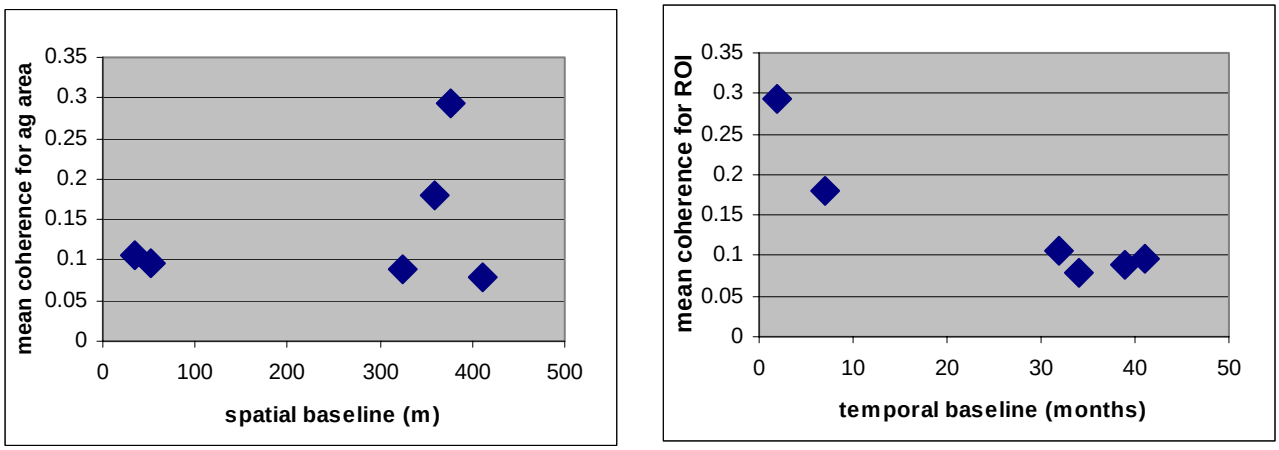

Figure 8. The relationship between the mean coherence values of the agricultural region of interest (ROI) for the six InSAR pairs and their corresponding spatial and temporal baselines.

The remainder of the results and analysis will focus primarily on the agricultural region. The interferogram with the highest coherence in this area (920611-920820) has a mottled phase pattern that does not appear to be related to surface displacement (Fig. 7a). It also shows no correspondence with topography, implying the pattern it is not due to errors in the DEM or estimating the spatial baseline and therefore, probably due to atmospheric phase delays. The interferogram with the next highest ROI coherence (950415-951111) has a phase structure consistent with surface displacement (Fig.7f). Therefore, this pair will be used to test the ability of InSAR to generate a surface displacement map for agricultural areas in SW Utah.

The first step in generating the 950415-951111 displacement map is reducing the phase noise with an adaptive filter. Next the filtered phase is *unwrapped*. This step removes the 360 degree phase cycles inherent in the interferogram by summing up (integrating) the phase into a continuous two-dimensional field. Areas where the phase is noisy and unreliable are not included in the phase unwrapping. In this implementation, pixels with a coherence value of 0.3 and below were not included in the unwrapping processes and thus, not assigned an unwrapped phase value. A relative displacement field is computed from the unwrapped phase using the relationship

$$displ_{LOS} = \frac{\phi_{displ}}{2\pi}\frac{\lambda}{2}$$

where $displ_{LOS}$ is the relative displacement in the direction of the radar line-of-sight (23º from vertical for ERS-1), ϕ_{displ} is the unwrapped phase due to displacement, and λ is the wavelength of the radar (5.6 cm for ERS-1). The relive displacement image is converted

to an absolute displacement image by locating stable areas of suspected zero displacement and adding or subtracting a constant to the relative field such that the stable areas indicate zero displacement. The absolute displacement image is then geo-referenced to produce an absolute displacement map.

The radar line-of-sight displacement map for the southern end of the Escalante Valley west of Newcastle is shown in Figure 9. Since there is no ground truth available for the time between the SAR acquisitions, the zero-displacement phase was assumed to be the dominant value within the valley. This corresponds to the green color in Figure 9. The colors with a negative value indicate a lowering of the surface between the two SAR acquisition on 1995/04/15 and 1995/11/11 while the positive values indicate a rising surface relative to the assumed surface of no change. The displacement map is shown over a gray-scale image of the near-infrared channel (band 4) of the Landsat ETM+ scene shown previously (Fig. 1). Band 4 was selected because it is most sensitive to photosyntheticly active vegetation, with the bright areas typically corresponding to healthy/dense vegetation. The image was constructed with an opaque displacement layer so that the underlying ground cover could be identified from the ETM+ layer. Areas without any color do not have a displacement value because the coherence was below the threshold level of 0.3 and therefore not unwrapped. The abrupt changes in color, particularly the large red areas in the Bull Valley Mountains (SW corner of Fig. 9) and the isolated blue spots in the north of the valley, are due to phase unwrapping errors and do not reflect changes on the surface.

It is not surprising that the coherence is low for many of the individual fields since the acquisitions probably span the growing and harvest seasons. Therefore, it is likely the condition, or even the presence, of the crops in these fields is different on the two acquisition dates. Several of the smaller *wholes* in the displacement map are coincident with individual circular fields (northwest corner of Fig. 9). The NW-SE trending road from Newcastle to Modena is evident because the coherence on either side changes abruptly in places.

The portion of the valley covered by the displacement map can be analyzed in detail. The red areas in the north-central part of the valley (near transects A and B) indicate the surface is rising, at least relative to the valley edges in the northeast (colored green and blue). Transects across this area show the surface is moving upwards about 2 cm from the east towards the west (Fig. 10). There is a trough in A-A' between location 300 and 350 where the surface is rising about 1 cm less than to either side. The spatial pattern of this feature is evident as the green area near C' in Figure 9. The orientation and shape of this displacement trough seems to correspond to the landscape patterns and texture seen in the Landsat image (Figs. 9 and 1). Transect C-C' also shows the valley floor rising about 2 cm relative to the bounding slope on the south at C (Fig. 11).

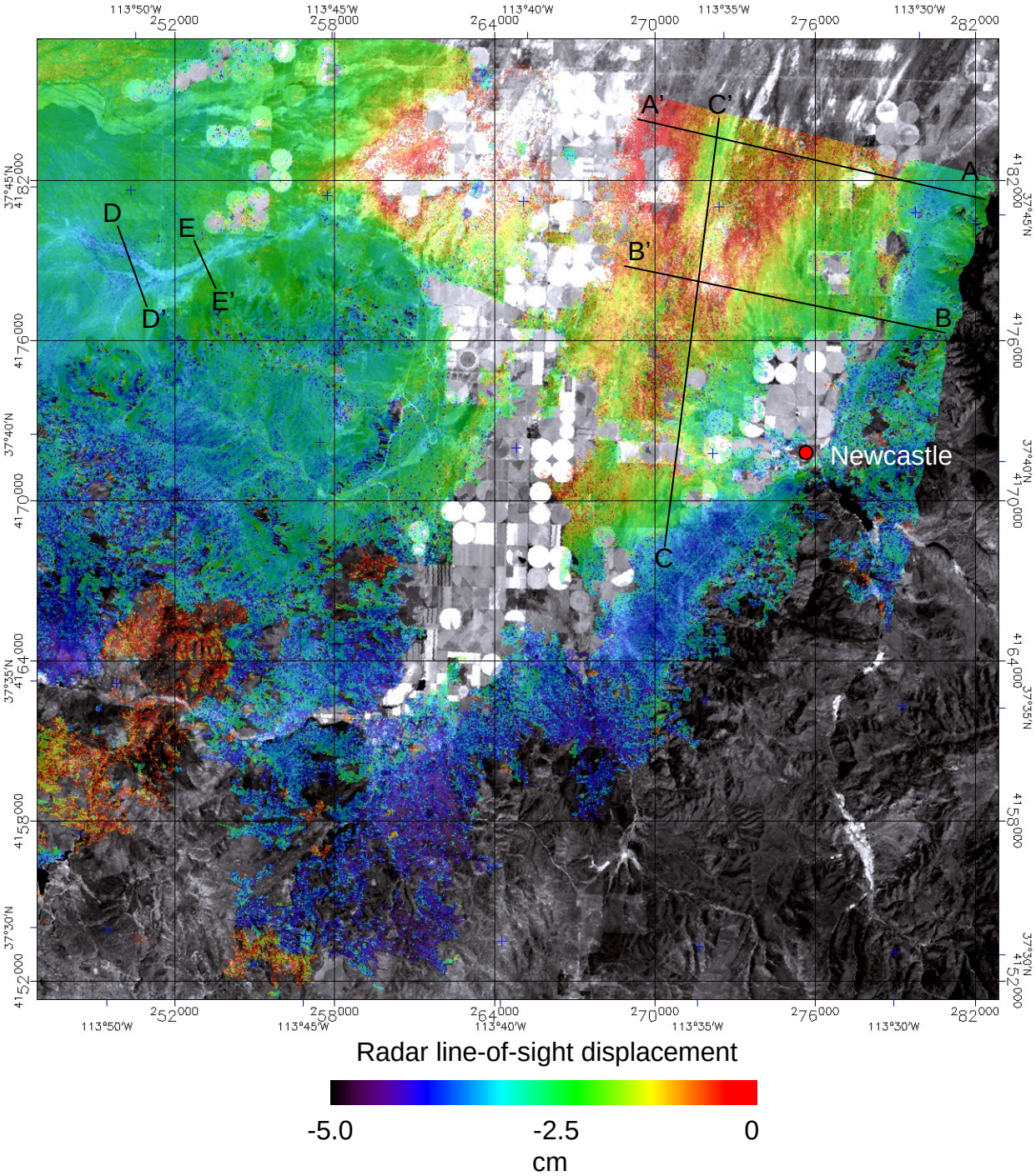

Figure 9. Radar line-of-sight displacement map from InSAR pair 950415-951111 in opaque color over Landsat ETM+ band 4 in gray-scale (Fig. 1). Negative values indicate surface lowering relative to an assumed stable surface assigned to zero displacement (red areas in center of valley). Transects A-E are shown in Figures 10-13. The abrupt changes in color, for example the large red areas in SW corner and the isolated blue spots in the north of the valley, are due to processing artifacts and do not reflect changes on the surface.

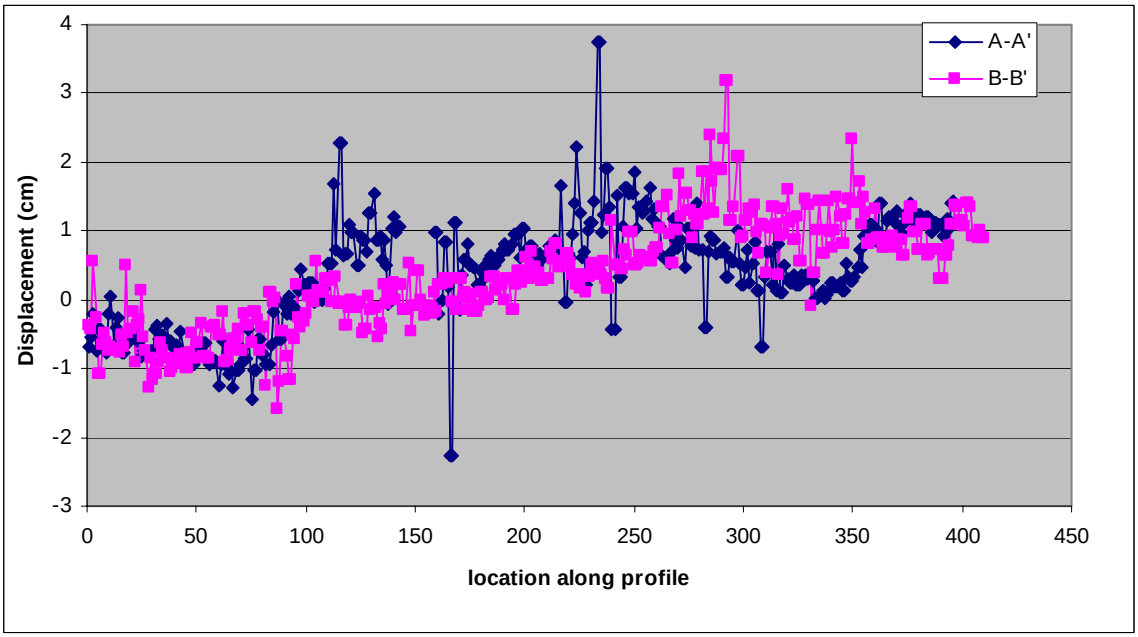

Figure 10. Displacement in the radar line-of-site along transects A-A' and B-B' with their location shown in Figure 9.

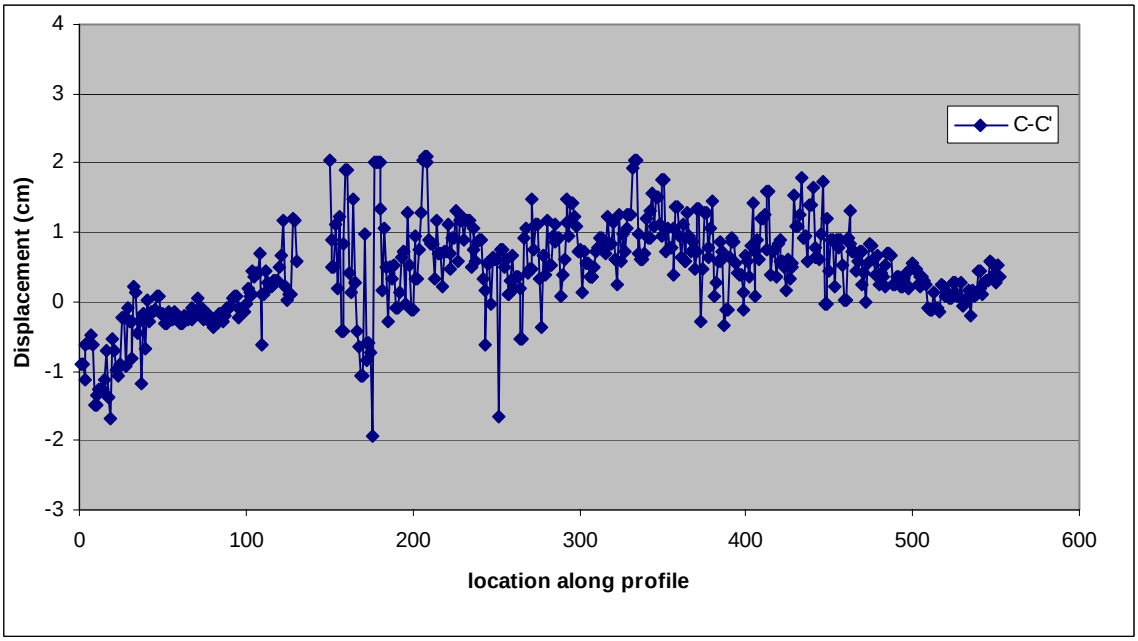

Figure 11. Displacement in the radar line-of-site along transect C-C' with the location shown in Figure 9.

The western part of the valley is more stable, characterized by little change in surface elevation in the vicinity of the agricultural fields. There is however an interesting feature in the displacement map just south and west of the circular fields (transects D and E) (Fig. 9). The narrow blue lineations in the displacement field coincide directly with a stream channel that is visible in the ETM+ band (Figs. 9 and 1). Transects across this channel indicate it has subsided approximately 8 mm between the two acquisitions. It is unlikely this is the result of simple channel scouring since the coherence would be lost if there was redistribution of the material in the stream bed.

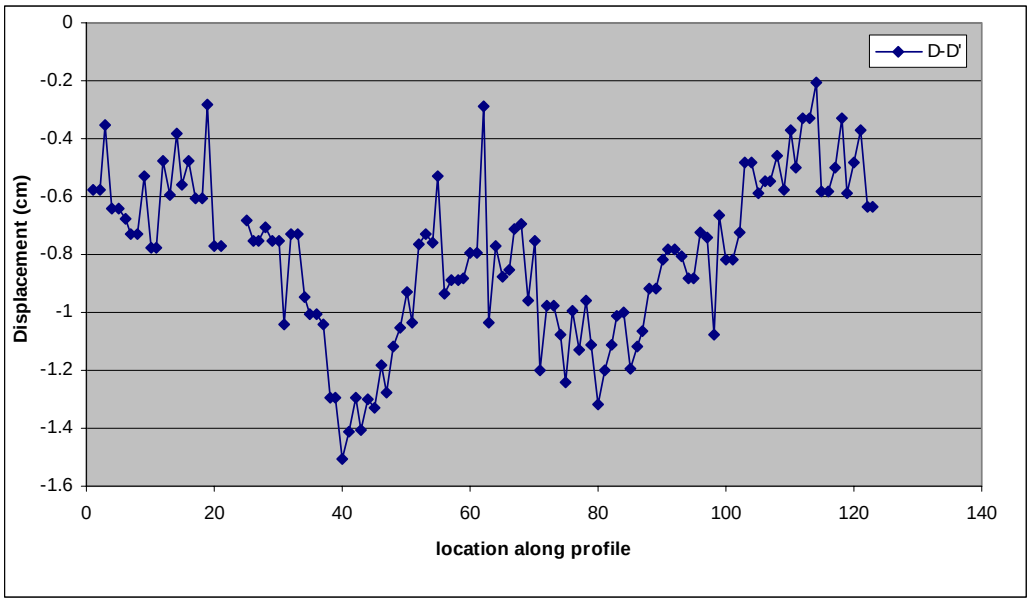

Figure 12. Displacement in the radar line-of-site along transect D-D' with the location shown in Figure 9

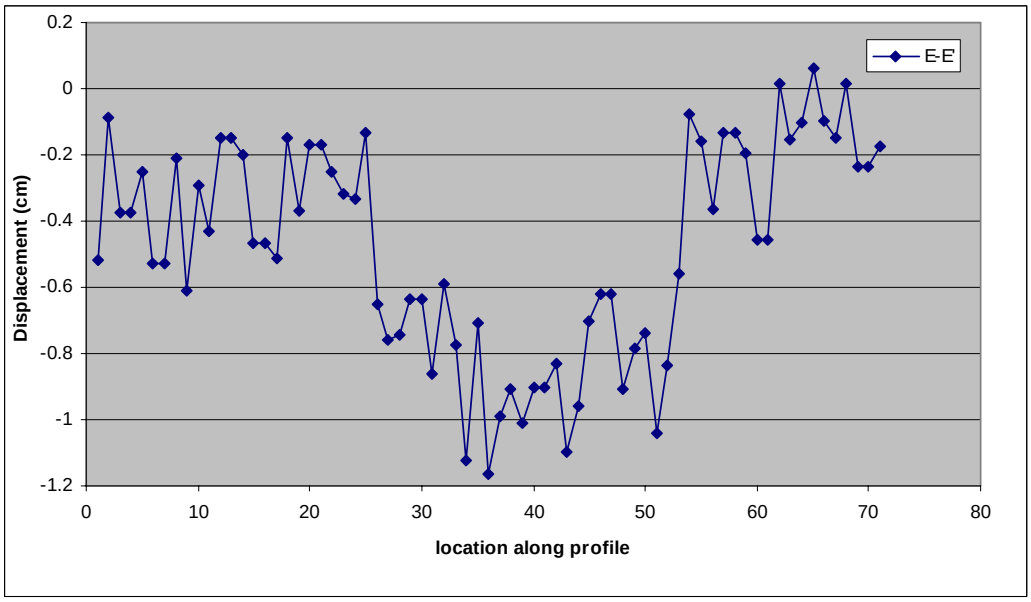

Figure 13. Displacement in the radar line-of-site along transect E-E' with the location shown in Figure 9.

A three-dimensional representation of the displacement map and the Landsat image was created by draping Figure 9 on the DEM using an interactive display in ENVI. This static visualization can assist with interpretations (Fig. 14), however the real power of the technique is in the dynamic interaction.

Conclusions and Implications for Phase-2

This section presents conclusions from this study (Phase-1) and their implications for a more extensive project (Phase-2).

In the agricultural portion of the radar images short temporal baselines produced high coherence values and a useable phase signal, even with long spatial baselines. The two InSAR pairs with the highest coherence in the agricultural ROI have temporal baselines of 2 and 7 months with spatial baselines of 376 and 359 m respectively (Table 3 and Fig. 8). A factor that may be as influential as the magnitude of the temporal baseline is the timing of two acquisitions relative to the growing season. The four pairs with low ROI coherence have one acquisition date during the growing season and the other during the dormant vegetation season (Table 3, Figs 4 and. 8). The two pairs mentioned above, with the highest ROI coherence and shortest temporal baselines (920611-960820 and 950415-95111), also happen to have paired acquisitions that fall within the same vegetation growth state. (This assumes the vegetation is not yet in a substantial growth stage by mid April). Therefore, with the Phase-1 data it is not possible to deconvolve the affects of the magnitude of the temporal baseline and the timing of the paired acquisitions. However, the baseline analysis from Phase-1 does imply spatial baselines approaching 400 m could be used in Phase-2 as long as the temporal baselines are either short or the paired acquisitions are in sync with the vegetation growth cycle. The highest coherence pair (920611-920820) also indicates that even summer pairs are useful if both are acquired during the same summer.

There are over 50 SAR scenes presently in the ESA archive for the frame that includes the Parowan Valley and Hurricane Cliffs. These acquisitions begin in 1992 and continue to the present. This magnitude of available scenes translates to over 1000 possible pairs. While this number of pairs does not need to be processed it implies there will be a wide variety of spatial and temporal baselines accessible. The list of acquisitions includes over 25% in the late fall/winter when vegetation influences should be minimized. There are also many pairs acquired within the same summer. A preliminary assessment of the spatial baselines indicates that about half of the pairs will have a baseline of < 400 m.

The displacement map created in Phase-1 demonstrates there is a fine-scale association of the measured surface motion with individual landscape features (Figs 9 and 1). The *trough* in the displacement map in the NE of the valley corresponds with the orientation and texture pattern evident in the Landsat image. The pattern of displacement in the west valley correlated directly with a stream channel. Even some of the locations of the gaps in the displacement map (due to low coherence) have a circular shape and are centered on individual center pivot irrigation fields. This correspondence of coherence levels and

most importantly, phase patterns with specific features in the Landsat image, gives confidence that InSAR derived displacement maps for southwest Utah are capable of measuring the subtle response of changes in land surface motion.

This confidence coupled with the numerous scenes available for the Parowan Valley area implies the following procedure could be used in Phase-2:
1. Produce a time series of sequential displacement maps (1992-present) using short temporal baselines (sub annually) to characterize any season signal present in the surface motion. If there is a surface response due to cyclical aquifer pumping and recharge this type of time series will allow it to be measured. Spatial and/or temporal changes in this pattern during the time series can also be measured.
2. The spatial pattern in any long-term change can be mapped by averaging or stacking the interferograms over the length of the time series. This averaging reduces atmospheric affects in the displacement maps. Any seasonal deformation pattern (from step 1 above) can be removed leaving the long-term trend.
3. Subtle changes in land cover, either natural or as the result of land use change, can easily be detected with the time series of coherence images.

This study also implies InSAR has the capability to map surface displacement in areas other than agricultural fields in southwest Utah. The previously mentioned relationship between baselines and coherence for the agricultural ROI is not the case for other portions of the SAR scenes. For example the pair with the longest temporal baseline (3 years, 5 months; Fig. 6c) has relatively high coherence over most of the scene outside of the agricultural area. This is probably due in part to the short spatial baseline of 52 m, however, the other pair with a temporal baseline > 3 yrs. (Fig. 6e) also has high coherence in non vegetated areas and its spatial baseline is 324 m. Therefore, the measurement of cm-scale surface motion in other non-agricultural areas over multiple-year time scales in southwest Utah appears possible. Potential applications include: landslides, soil creep, subsidence to mining, oil and gas extraction, or changes due to subsurface water injection.

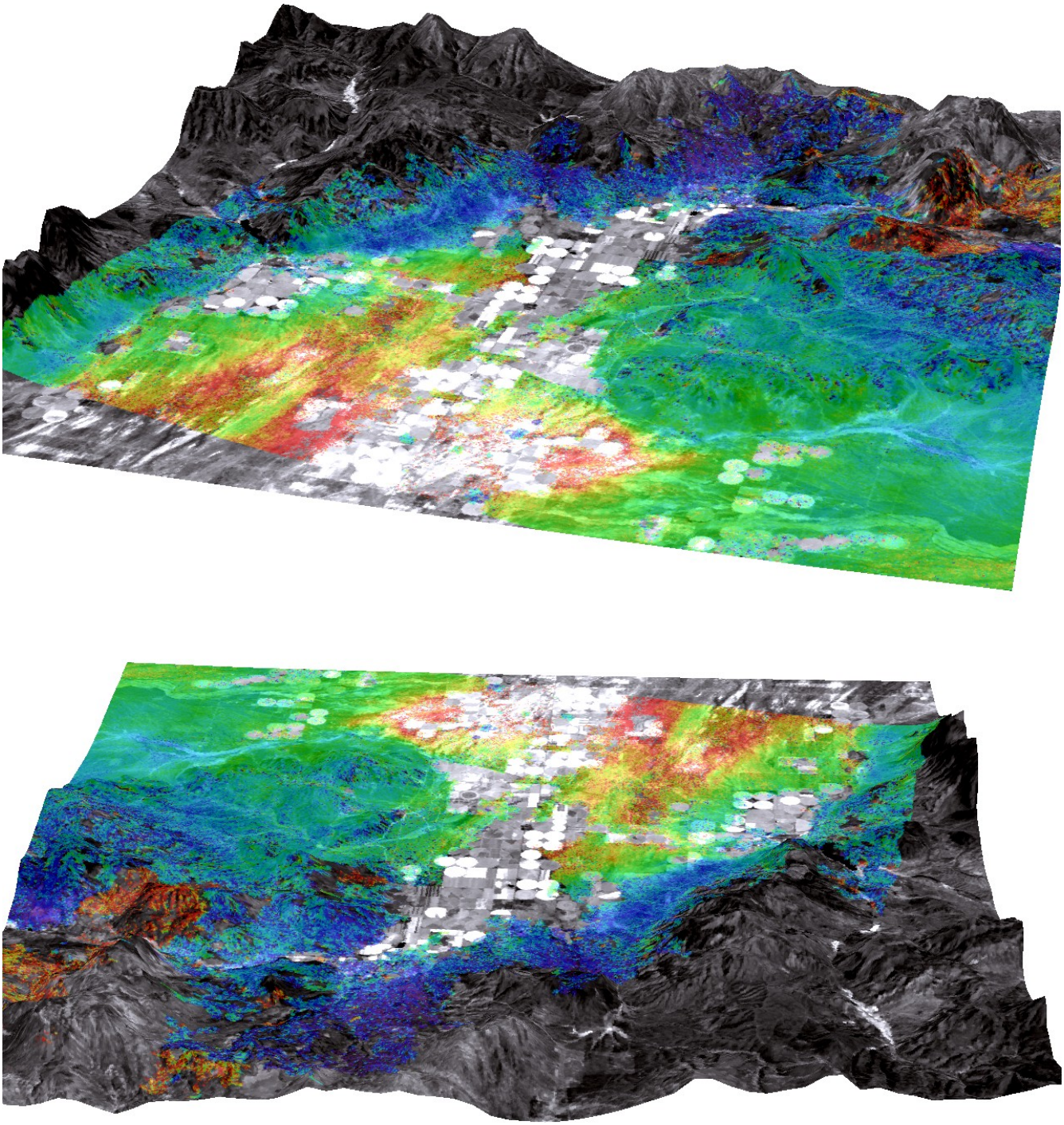

Figure 14. Three-dimensional visualization of Figure 9 using the USGS DEM with a vertical exaggeration of 7x looking toward a) the southeast and b) the north.